Sequential Drug Release and Enhanced Photothermal and Photoacoustic Effect of Hybrid Reduced Graphene Oxide-Loaded Ultrasmall Gold Nanorod Vesicles for Cancer Therapy

Jibin Song,[†,‡] Xiangyu Yang,[‡] Orit Jacobson,[‡] Lisen Lin,[‡] Peng Huang,[‡] Gang Niu,[‡] Qingjie Ma,[*,†] and Xiaoyuan Chen[*,‡]

[†]China-Japan Union Hospital of Jilin University, Changchun, Jilin 130033, China and [‡]Laboratory of Molecular Imaging and Nanomedicine (LOMIN), National Institute of Biomedical Imaging and Bioengineering (NIBIB), National Institutes of Health, Bethesda, Maryland 20892, United States

ABSTRACT We report a hybrid reduced graphene oxide (rGO)-loaded ultrasmall plasmonic gold nanorod vesicle (rGO-AuNRVe) (~65 nm in size) with remarkably amplified photoacoustic (PA) performance and photothermal effects. The hybrid vesicle also exhibits a high loading capacity of doxorubicin (DOX), as both the cavity of the vesicle and the large surface area of the encapsulated rGO can be used for loading DOX, making it an excellent drug carrier. The loaded DOX is released sequentially: near-infrared photothermal heating induces DOX release from the vesicular cavity, and an intracellular acidic environment induces DOX release from the rGO surface. Positron emission tomography imaging showed high passive U87MG tumor accumulation of ^{64}Cu-labeled rGO-AuNRVes (~9.7% ID/g at 24 h postinjection) and strong PA signal in the tumor region. Single intravenous injection of rGO-AuNRVe-DOX followed by low-power-density 808 nm laser irradiation (0.25 W/cm^2) revealed effective inhibition of tumor growth due to the combination of chemo- and photothermal therapies. The rGO-AuNRVe-DOX capable of sequential DOX release by laser light and acid environment may have the potential for clinical translation to treat cancer patients with tumors accessible by light.

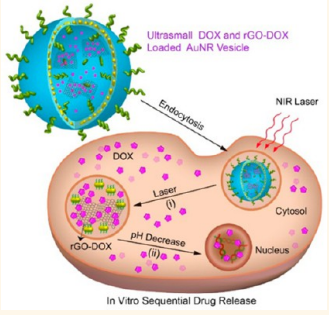

KEYWORDS: hybrid nanovesicle · sequential release · photothermal effect · photoacoustic imaging · PET imaging

Plasmonic metal nanocrystals with localized surface plasmon resonance (LSPR), a widely explored theranostic platform, have been applied to biosensing, bioimaging, photothermal therapy, and drug delivery.[1−5] The LSPR wavelength of plasmonic metal nanoparticles can be tuned from the visible to the NIR region by adjusting their shape, size, composition, or interparticle distance.[6−8] Among these, tuning interparticle spacing is the most effective approach to adjust the LSPR spectrum of the plasmonic nanostructure.[6] Thus, diverse plasmonic assemblies with strong interparticle plasmonic coupling have been developed as excellent bioimaging and photothermal agents for image-guided cancer therapy.[9−14] We previously developed plasmonic vesicles assembled from gold nanocrystals, with enhanced photothermal effect and photoacoustic (PA) signal due to the strong plasmonic coupling of the gold nanocrystals in the vesicular shell.[10] However, the relatively large size (>200 nm) of the vesicle limits its application by local administration.[9] Furthermore, the previously reported gold nanorods (AuNR) used for assembly of nanovesicles usually have a length of over 40 nm and a width of over 8 nm, resulting in undesired accumulation into the reticuloendothelial system (RES) and slow clearance from the body.[15,16]

Reduced graphene oxide (rGO) nanoparticles with a large surface area for drug loading and photothermal effect for photothermal therapy have been widely explored for theranostic applications.[17,18] Both hydrophobic and hydrophilic aromatic anticancer drugs can be loaded onto the rGO surface *via* $\pi-\pi$ stacking or hydrophobic−hydrophobic

* Address correspondence to (Q. Ma) maqingjiejlu@163.com, (X. Chen) shawn.chen@nih.gov.

Received for review June 22, 2015 and accepted August 26, 2015.

Published online August 26, 2015
10.1021/acsnano.5b03804

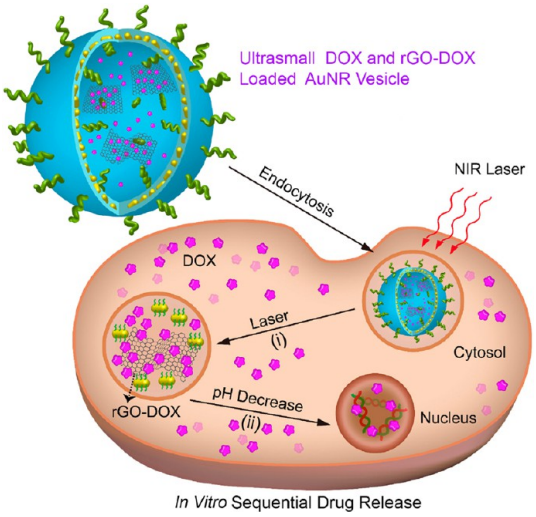

Scheme 1. Schematic illustration of sequential DOX release triggered by (i) remote NIR laser irradiated photothermal effect and (ii) acidic environment of the cancer cell.

interactions.[17] Apart from its nature of being an excellent drug carrier, rGO can also serve as a photothermal agent and convert the absorbed light into heat, thus inducing hyperthermia to the cancer cells or surrounding tissue.[19] Although rGO can absorb light from the UV to NIR region and subsequently release it as heat by nonradioactive decay, the broad absorption spectrum and low quantum efficiency of rGO have relatively low photothermal conversion efficiency.[20,21] It was recently reported that the photothermal performance of rGO can be increased after being coated on a plasmonic nanoparticle surface or when the plasmonic nanoparticle is anchored on the rGO surface. The enhanced photothermal effect is due to the fact that the plasmonic nanoparticles act not only as photothermal source but also as local nanoantennae to increase the light absorption efficiency of rGO at the plasmon frequency of the nanoparticle.[22,23]

In the current study, we developed a new kind of carbon−metal hybrid rGO-conjugated DOX (rGO-DOX)-loaded ultrasmall plasmonic gold nanorod vesicle (rGO-AuNRVe-DOX) for integrated chemo-photothermal therapy (Scheme 1). The rGO-AuNRVe (~74 nm in size) was prepared by assembling amphiphilic small AuNRs (dimension: ~9 × 2 nm) grafted with poly(ethylene glycol) (PEG), poly(lactic-*co*-glycolic acid) (PLGA), and PEGylated rGO using a double-emulsion method. The encapsulation of rGO-DOX in the AuNRVe avoids direct interaction of rGO-DOX with the physiological environment during the circulation and cellular internalization of DOX. The rGO-AuNRVe exhibits remarkable enhancement of the photothermal effect and PA signal compared with the single AuNR and the mixture of rGO and AuNRVe, resulting from the plasmonic coupling of the conjugated small AuNRs in the vesicular shell and the interaction of the encapsulated rGO and plasmonic shell. Zhang *et al*. reported that the inside of a plasmonic metal shell can behave as a cavity where electromagnetic radiations are concentrated, leading to increased light absorption efficiency of the encapsulated rGO.[24] The accumulation of the hybrid vesicle in the tumor region after intravenous injection into U87MG tumor-bearing mice leads to a dramatic increase of the PA signals. Positron emission tomography (PET) imaging results showed that the ^{64}Cu-labeled hybrid vesicle reached ~9.7% ID/g in the tumor region at 24 h postinjection. For integrated chemo-photothermal therapy, relatively low laser power density (808 nm, 0.25 W/cm^2) irradiation leads to a mild increase of tumor temperature, which is sufficient to disrupt the rGO-AuNRVe-DOX and sequential release of rGO-DOX and DOX from the vesicle. The elevated temperature also brings about enhanced intracellular uptake of DOX. Our *in vivo* experiment results showed that the hybrid rGO-AuNRVe-DOX demonstrated high cancer therapy efficacy due to the synergistic effect of photothermal therapy and controlled release of chemotherapeutics.

RESULTS AND DISCUSSION

Preparation of Hybrid rGO-Loaded Ultrasmall Gold Nanorod Vesicles. To prepare ultrasmall AuNRVes, small AuNRs (~9 × 2 nm) (Figure S1) were first synthesized using a seedless method.[25] The small AuNRs were further coated with a hydrophilic polymer brush of PEG (M_n = 5 kDa) and a hydrophobic polymer brush of PLGA (M_n = 7.2 kDa) (AuNR@PEG/PLGA) *via* a ligand exchange method by forming covalent Au−S bonds (Figure S2).[10] Each amphiphilic AuNR@PEG/PLGA carries an average of 12 PEG and 12 PLGA brushes, calculated from a molar ratio of PEG:PLGA = 1:1, and the weight fraction of the polymer weight is 31.5% (see Supporting Information for details). The vesicle was prepared by using a water-in-oil-in-water (W_1/O/W_2) double-emulsion, oil solvent-diffusion-evaporation method, which is a commonly used approach to prepare polymer vesicles.[26] To encapsulate rGO (30−120 nm) into the cavity of the vesicle, the hydrophilicity of rGO was first increased by conjugating PEG (M_n = 2 kDa) *via* an amide bond (rGO-PEG), as shown in Figures 1a and S3. Thus, the rGO-loaded hybrid vesicle was prepared by self-assembly of rGO-PEG in water (internal aqueous phase, W_1) and AuNR@PEG/PLGA in oil under sonication (see Supporting Information for details). The as-prepared rGO-AuNRVes were purified by centrifugation and washed with deionized water three times to remove unloaded rGO-PEG. The SEM image showed that the vesicles were spherical in shape with a monolayer of AuNR in the vesicle shell (Figure 1b). The TEM image of rGO-AuNRVe does not allow a clear identification of the rGO once it is loaded into the vesicle, due to the lower contrast compared with the AuNR shell (Figure 1c). After disassembling the hybrid vesicle, rGO was released from the vesicular

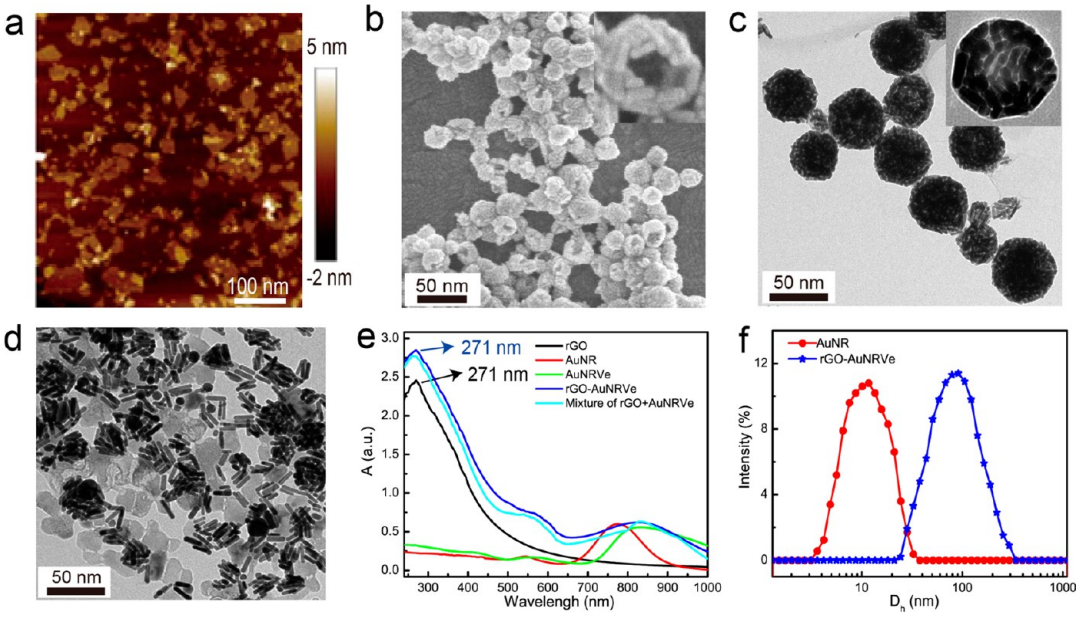

Figure 1. (a) AFM image of PEGylated reduced graphene oxide (rGO-PEG). (b) SEM and (c) TEM images of the rGO-loaded ultrasmall gold nanorod vesicle (rGO-AuNRVe). (d) TEM image of disassembled rGO-AuNRVe. (e) UV−vis spectra of the aqueous solution of rGO-PEG, small AuNR@CTAB, AuNRVe, a mixture of rGO and AuNRVe, and rGO-AuNRVe. (f) Hydrodynamic diameter distribution of small AuNR@CTAB and rGO-AuNR-Ve in aqueous solution.

cavity, and its detection was thus clearly displayed in the TEM image (Figure 1d). Due to the plasmonic coupling of the AuNRs in the vesicular shell, both the longitudinal and transverse LSPR of the AuNR were remarkably red-shifted (Figure 1e).[27] The rGO was also identifiable from the UV−vis spectra of the rGO-AuNRVe as compared with pure AuNRVe. The average size of the rGO-AuNRVe was 65 ± 12.6 nm, as demonstrated by dynamic light scattering measurement (Figure 1f). As a control experiment, poly(methyl methacrylate-*co*-4-vinylpyridine) with 25% 4-vinylpyridine (4VP, pK_a = 5.4) (PMMAVP) was attached to the AuNR surface as the hydrophobic grafts, creating pH-responsive AuNR coated with PEG and PMMAVP (AuNR@PEG/PMMAVP). We further prepared a pH-responsive rGO-loaded AuNRVe by self-assembly of AuNR@PEG/PMMAVP and rGO-PEG, which is stable at pH 7.4 and disassembles at pH 5.0 (see Supporting Information for details).[12] Once the pH-responsive rGO-AuNRVes were dispersed in a pH 5.0 aqueous solution, the vesicles were disrupted into small clusters or single AuNRs, and the released rGO was observed in the TEM image (Figure S4).

Photothermal and Photoacoustic Properties of the Hybrid rGO-Loaded Ultrasmall Gold Nanorod Vesicle. To demonstrate the enhanced photothermal effect, the hybrid rGO-AuNRVes in water at a concentration of 0.1 mg/mL were exposed to an 808 nm laser at a power density of 0.25 or 0.5 W/cm^2 for 5 min, respectively. Temperature variations of the solution were recorded using an infrared camera (Figure S5). The temperature of the hybrid vesicle solution was rapidly increased to more than 76 °C, higher than that observed in the mixture of rGO and AuNRVe, which reached 65 °C under the same conditions (Figure 2a), which can be ascribed to the interaction between the loaded rGO and the plasmonic shell, leading to an increased light absorption of rGO when irradiated with an NIR laser.[23] Water alone showed almost no heating effect. Figure 2b showed that the temperature of the hybrid vesicle solution increased with the increasing power density of the exposed laser (Figure 2b). The photothermal conversion efficiency of the rGO-AuNRVe was 63% based on our previously reported calculation method, which is higher than AuNRVe (~51%).[9]

We further examined the PA performance of the hybrid rGO-AuNRVe, AuNRVe, AuNR, and the mixture of rGO and AuNRVe illuminated with an 808 nm laser. The rGO-AuNRVe displayed a stronger PA signal than the mixture of rGO and AuNRVe based on the same OD_{808} value (Figure 2c). As shown in Figure 2d, the PA intensities of all the samples in aqueous solution increased linearly with increasing OD_{808} values. At OD_{808} = 1, the PA intensity of rGO-AuNRVe was about 2.5 times higher than that observed in the mixture of rGO and AuNRVe. Despite the presence of rGO-PEG in AuNRVe aqueous solution, the mixture of rGO and AuNRVe showed similar PA signal amplitude to that of AuNRVe at the same OD_{808} value. The remarkable enhancement of the PA signal amplitude of the hybrid rGO-AuNRVe is suitable for further *in vivo* PA imaging applications, because the minimum concentration of rGO-AuNRVe required for PA-based diagnosis can be dramatically reduced.[28]

Sequential Drug Release of Hybrid rGO-DOX and DOX-Loaded Gold Nanorod Vesicles. We next investigated the use of

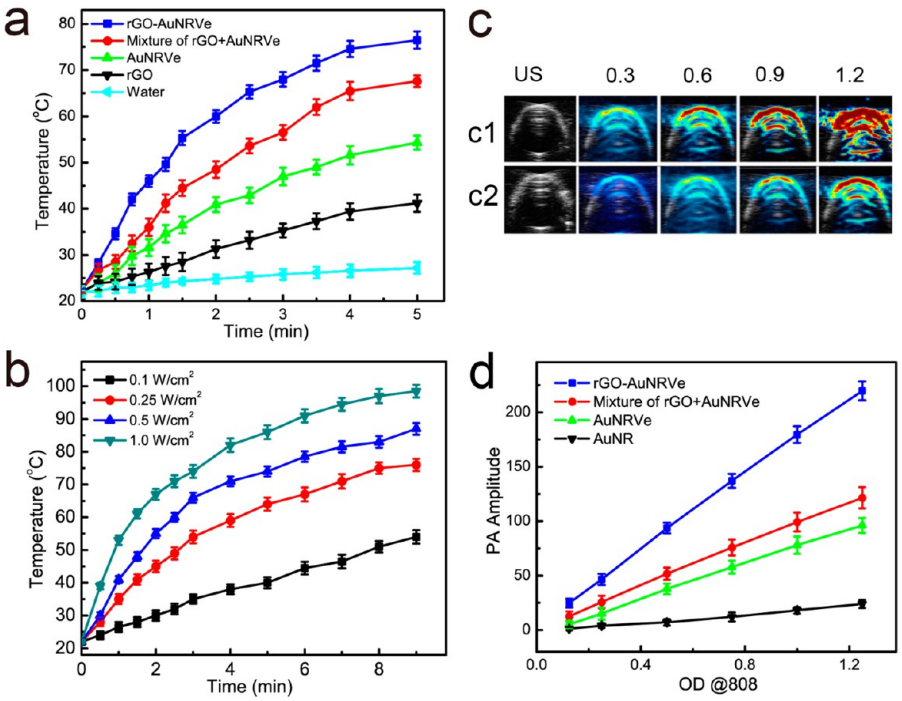

Figure 2. Characterization of rGO-AuNRVe by photothermal and photoacoustic (PA) studies. (a) Temperature changes of water, rGO, AuNRVe, a mixture of rGO and AuNRVe, and rGO-AuNRVe irradiated with an 808 nm laser at a power density of 0.5 W/cm^2 as a function of time. (b) Temperature variations of rGO-AuNRVe irradiated with an 808 nm laser at different power densities. (c) PA images of rGO-AuNRVe (c1) and mixture of rGO and AuNRVe (c2) of different OD_{808} values. (d) PA intensities of the aqueous solution of AuNR, rGO, rGO-AuNRVe, and a mixture of rGO and AuNRVe as a function of OD_{808} values.

hybrid rGO-AuNRVe for loading and release of anticancer drugs. Due to the ultrahigh polyaromatic surface area, rGO can have a high loading content of aromatic drug molecules by $\pi-\pi$ stacking and hydrophobic−hydrophobic interaction.[29,30] To combine the DOX loading abilities of rGO and AuNRVe, we prepared DOX and PEGylated rGO-DOX-loaded hybrid vesicle. PEG-modified rGO is stable in aqueous solution, especially in physiological environment.[31] The DOX-loaded hybrid vesicle was prepared by using the same $W_1/O/W_2$ double-emulsion method in the presence of DOX and rGO-PEG-DOX in W_1. Successful loading of rGO-DOX and DOX in the hybrid vesicle was demonstrated by the UV−vis absorbance spectra of the samples (Figure 3a). After loading DOX and rGO-DOX, rGO-AuNRVe-DOX displayed characteristic absorption peaks of DOX at 485 nm and rGO at 271 nm, respectively.[32] The DOX loading content of DOX-rGO-AuNRVe reached 65%, which is about 3 times higher than that of DOX-AuNRVe. Indeed, large amounts of rGO with ultrahigh loading content of DOX were encapsulated into the vesicle together with free DOX (Figure 3b). Due to the fluorescence quenching effect of rGO and the plasmomic AuNR shell to the conjugated DOX, the fluorescence signal of DOX-loaded rGO-AuNRVe was substantially reduced compared with free DOX at the same concentration (Figure S6), which further confirmed the successful preparation of rGO-AuNRVe-DOX.

The DOX release ability triggered by NIR laser photothermal heating and acid was further investigated. Upon laser irradiation, the integrity of the vesicle was disrupted, causing rapid release of the encapsulated DOX in the cavity of the hybrid vesicle. The DOX on the rGO surface was subsequently released in the acid environment. Our results showed that the rGO-AuNRVe-DOX irradiated with 808 nm laser at a power density of 0.25 W/cm^2 released about 30% percent of the loaded DOX at pH 7.4 (Figure 3c). However, no DOX was further released from the rGO-AuNRVe-DOX over time postirradiation, indicating that the partially released DOX was from the cavity of the vesicle and not from the rGO surface. To further confirm this hypothesis, the pH value of the solution was adjusted to 5.0 by adding 1 M HCl into the solution at 70 min postirradiation (Figure 3c). More DOX was readily released, and over 80% of DOX was finally released at the 10 h time point. On the other hand, much less DOX (<8%) was released by the rGO-AuNRVe-DOX without laser irradiation or when dispersed in a pH 5.0 solution. As shown in Figure 3d, the fluorescence intensity of rGO-AuNRVe-DOX at pH = 5.0 after laser irradiation was approximately 3 times higher than that displayed at pH = 7.4, thereby suggesting that more DOX was released in an aqueous solution at pH = 5.0. Without laser irradiation, rGO-AuNRVe-DOX displayed a negligible fluorescence signal in an aqueous solution at both pH = 5.0 and pH = 7.4, indicating that little to no DOX was released from the DOX-loaded hybrid vesicle. These results suggest that rGO-AuNRVe-DOX possesses a sequential drug release behavior, one

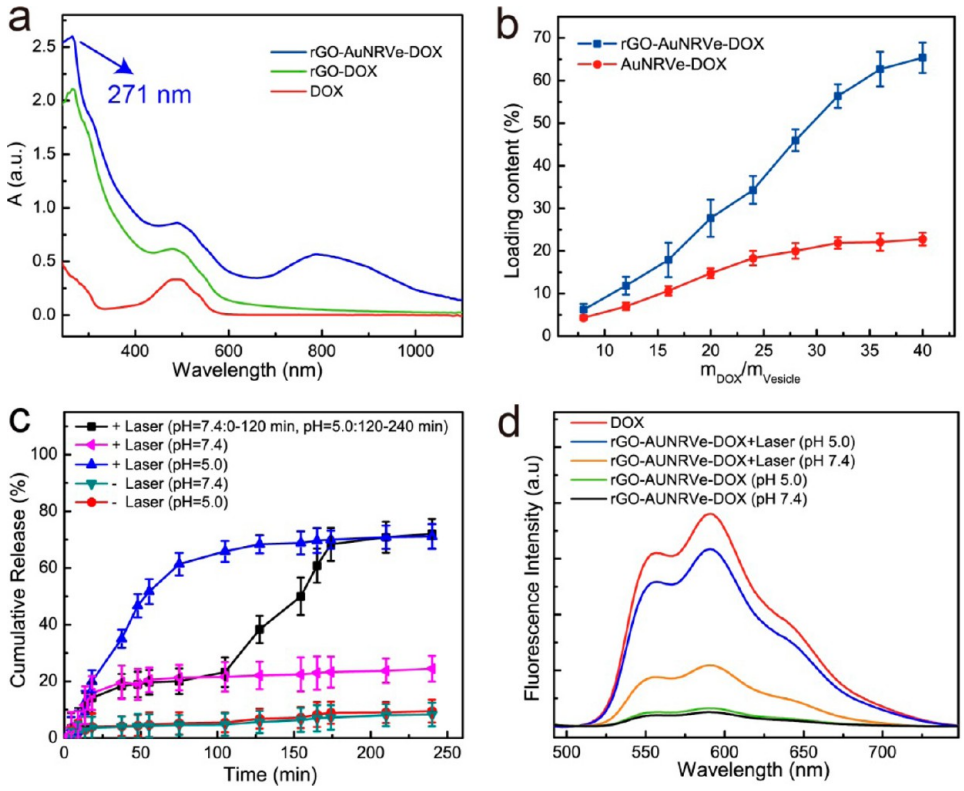

Figure 3. (a) UV−vis spectra of free DOX, PEGylated rGO-DOX, and DOX-loaded small AuNR@PEG/PLGA vesicle. (b) Loading content of rGO-AuNRVe-DOX and AuNRVe-DOX. (c) Stimuli-responsive DOX release profiles of different samples irradiated with or without NIR laser irradiation in pH = 5.0 or pH = 7.4 aqueous solution. (d) Fluorescence spectra of free DOX and rGO-AuNRVe-DOX treated with or without NIR laser irradiation in pH = 5.0 or pH = 7.4 aqueous solution.

depending on NIR laser photothermal heating and the other on the acidity. The NIR laser-dependent DOX release (first stage) may be used as an "on-demand" and remotely controlled drug release platform. More importantly, the second stage of DOX release is acid dependent, thus facilitating its application in cancer treatment since the tumor microenvironment is intrinsically acidic. In contrast, DOX was continuously released from the pH-responsive AuNR@PEG/PMMAVP control vesicle in an aqueous solution at pH = 5.0, thus exhibiting one-stage DOX release behavior, since the acid environment triggered both the disruption of the vesicle and the DOX release from the rGO surface (Figure S7).

Sequential Drug Release and Combined Chemo-photothermal Therapy by DOX-Loaded Hybrid Vesicles *in Vitro*. To investigate the photothermal therapeutic (PTT) effect of the rGO-AuNRVe on cancer cells *in vitro*, U87MG cancer cells were incubated with rGO-AuNRVe (0.1 mg/mL) for 3 h and subsequently washed with fresh medium. The cells were then irradiated with an 808 nm laser at a power density of 0.25 and 0.5 W/cm^2 for 5 min. The PTT effects were analyzed using live and dead cell staining assays with Calcein-AM (green color: live cells) and propidium iodide (PI) (red color: dead cells). Most of the cells were dead after a 0.25 W/cm^2 laser treatment (Figure S8a). When the laser power density was increased to 0.5 W/cm^2, complete cell death was observed within the laser spot. In contrast, the cells treated with AuNRVe and an 808 nm laser at 0.5 W/cm^2 induced a much lower PTT effect than those treated with rGO-AuNRVe. Without laser irradiation, cells treated with rGO-AuNRVe showed no cytotoxicity, indicating the biocompatibility of the hybrid vesicle. Furthermore, cell counting kit-8 (CKK-8) was used to quantify the cell-killing efficiency of rGO-AuNRVe and AuNRVe irradiated with an 808 nm laser at different power densities (Figure S8b). Cells treated with rGO-AuNRVe and AuNRVe both exhibited decreased cell viability with increasing 808 nm laser power density. However, the cells treated with rGO-AuNRVe required a remarkably lower laser power density than the cells with AuNRVe to obtain the same cell-killing effect. The cells treated with the hybrid vesicle of various concentrations (0.35−2.4 nM) up to 240 min of incubation without laser irradiation showed more than 95% viability (Figure S9), suggesting the excellent biocompatibility of the vesicle.

To investigate the *in vitro* DOX release behavior, U87MG cancer cells were incubated with rGO-AuNRVe-DOX for 3 h, washed with fresh medium, and observed by a fluorescence microscope. The cells showed a very weak fluorescence signal (Figure 4a (a1)), due to the quenching of DOX fluorescence by the plasmonic vesicle shell and rGO. Once the cells were irradiated with 0.25 W/cm^2 for 3 min, the red fluorescence signal of DOX was observed in both the cytosol and nucleus

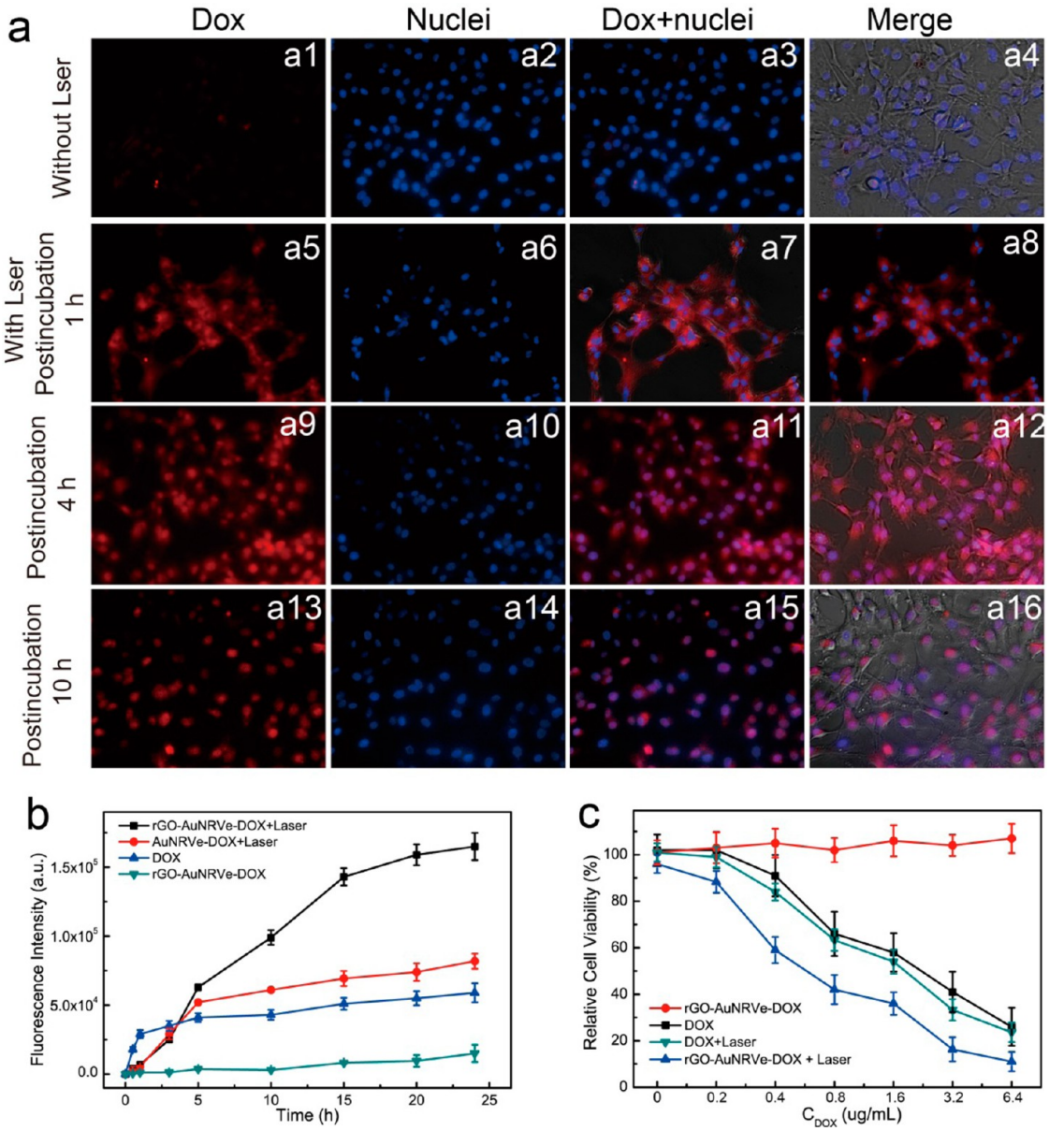

Figure 4. (a) Fluorescence, bright-field, and overlaid images of U87MG cells treated with small rGO-AuNRVe-DOX after 3 h incubation (a1−a4) and postincubation for 1 h (a5−a8), 4 h (a9−a12), and 10 h (a13−a16) after laser irradiation at 0.25 W/cm^2 for 3 min. (b) Fluorescence intensity changes of cells treated with rGO-AuNRVe-DOX with or without laser irradiation, AuNRVe-DOX with laser irradiation, and free dox as a function of incubation time. (Laser irradiation was carried out at 3 h postincubation with samples.) (c) Cell viability of U87MG cancer cells treated with rGO-AuNRVe-DOX and DOX with and without 808 nm laser irradiation at a power density of 0.25 W/cm^2.

after incubation for 1 h (Figure 4a (a5−a8)), indicating that DOX was released from the vesicle. The cytosol still exhibited a strong fluorescence signal when the incubation time was increased to 4 h, suggesting that DOX was continuously released from the surface of rGO triggered by the intracellular acid environment (Figure 4a (a9−a12)). To further verify our results, the cells were incubated with AuNRVe-DOX vesicle without loading rGO-DOX and underwent the same treatment. The DOX was mainly localized in the nuclei, and no DOX fluorescence was observed in the cytosol between 1 and 4 h postincubation after laser irradiation (Figure S10). Taken together, these results showed that DOX in rGO-AuNRVe-DOX is sequentially released by NIR photothermal heating and by acid.

As shown in Figure 4b, the fluorescence intensity of the cells treated with rGO-AuNRVe-DOX and laser irradiation increased with time. However, no fluorescence signal was observed in the cells incubated with rGO-AuNRVe-DOX without laser irradiation. Furthermore, DOX was continuously released from the rGO-DOX surface of the rGO-AuNRVe-DOX, leading to an enhanced fluorescence signal when compared with AuNRVe-DOX, where no fluorescence intensity was observed at 5 h after laser irradiation. During the first 2 h incubation, the cells treated with free DOX showed

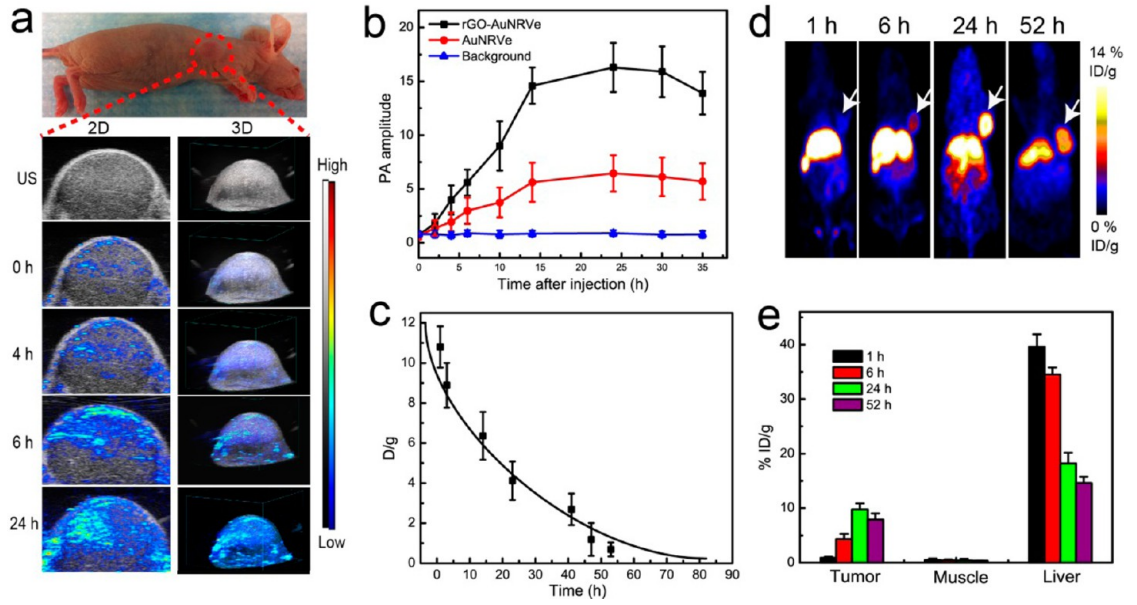

Figure 5. *In vivo* **ultrasound (US) photoacoustic (PA) 2D and 3D images (a) and intensities (b) of the U87MG tumor region at different time points after intravenous injection of rGO-AuNRVe. (c) Time-active curves of the biodistribution of radiometal [^{64}Cu]-labeled rGO-AuNRVe in the blood. (d) Decay-corrected whole-body coronal PET images of U87MG tumor-bearing mice at 1, 6, 24, and 52 h after intravenous injection of 150 μCi of [^{64}Cu]-labeled rGO-AuNRVe. (e) Biodistribution of rGO-AuNRVe in tumor, muscle, and liver at various time points postinjection of 150 μCi of [^{64}Cu]-labeled rGO-AuNRVe.**

a rapid fluorescence increase due to the simple diffusion of DOX through the cell membrane. The sequential drug release behavior of rGO-AuNRVe-DOX could efficiently increase the drug uptake and prolong the chemotherapy effect. As rGO is capable of loading different aromatic anticancer drugs, siRNA, and photosensitized agents, we believe that rGO-AuNRVe would serve as a multifunctional delivery platform for combined photothermal therapy and drug/gene delivery, potentially better than rGO alone.[17,29]

Encouraged by the enhanced photothermal effect and high drug-loading ability of rGO-AuNRVe, DOX was used as a model to test the potential of rGO-AuNRVe-DOX for chemo-photothermal therapy. The U87MG cancer cells were incubated with rGO-AuNRVe-DOX and free DOX at the same DOX concentration for 3 h and washed with fresh cell culture medium. Upon 808 nm laser irradiation (0.25 W/cm^2), the half-maximal inhibitory concentration (IC_{50}) of rGO-AuNRVe-DOX was ~0.63 μg/mL, which was approximately 2 times lower than that of free DOX (~1.34 μg/mL) (Figure 4c). However, without laser irradiation, rGO-AuNRVe-DOX showed no toxicity due to nearly no DOX release. As rGO-AuNRVe irradiated with a 0.25 W/cm^2 laser showed rather low cytotoxicity, there is a synergy between the photothermal therapy from rGO-AuNRVe and chemotherapy from the released DOX that is considerably better than either treatment alone.

***In Vivo* Photoacoustic (2D and 3D) and PET Imaging by Hybrid Vesicles.** To improve the cancer therapy efficacy, a series of imaging methods and agents had been developed for imaging during therapy.[33−35] Encouraged by the strong PA signal of the hybrid rGO-AuNRVe, we investigated its use as an PA contrast agent by using U87MG tumor-bearing mice. When the tumor volume reached ~60 mm^3, 200 μL of rGO-AuNRVe in PBS (0.5 mg/mL) was injected intravenously into the mice. Figure 5a shows the two-dimensional (2D) and three-dimensional (3D) images of the tumor section at different time points after intravenous injection of the sample. PA signal in the tumor region increased with increasing time after injection and reached the maximum value at 24 h postinjection. The strong 3D PA signal showed the whole morphology and shape of the tumor, which is consistent with the ultrasound image. The average PA intensity of the tumor was also increased as a function of time. The PA intensity of the tumor treated with AuNRVe was 4 times lower than that of the rGO-AuNRVe at 24 h postinjection (Figure 5b). The results suggest rGO-AuNRVe as an excellent PA imaging probe to track the tumor accumulation of the vesicle and to provide information regarding tumor parameters (*i.e.*, size and shape), which is essential to adjust the laser spot size and power density of photothermal therapy to reach the best performance.[36]

PET imaging with a high target sensitivity can quantify the biodistribution of the samples *in vivo*, which had been successfully used in the clinic.[37] To test the *in vivo* distribution of the hybrid vesicle using PET, a radiometal ^{64}Cu-labeled hybrid vesicle was prepared based on our previously reported chelator-free method[37,38] and injected intravenously into U87MG tumor-bearing mice. Our results showed that the *in vivo* half-time circulation of the ^{64}Cu-labeled vesicle was ~19.6 h (Figure 5c), due to the ~65 nm size

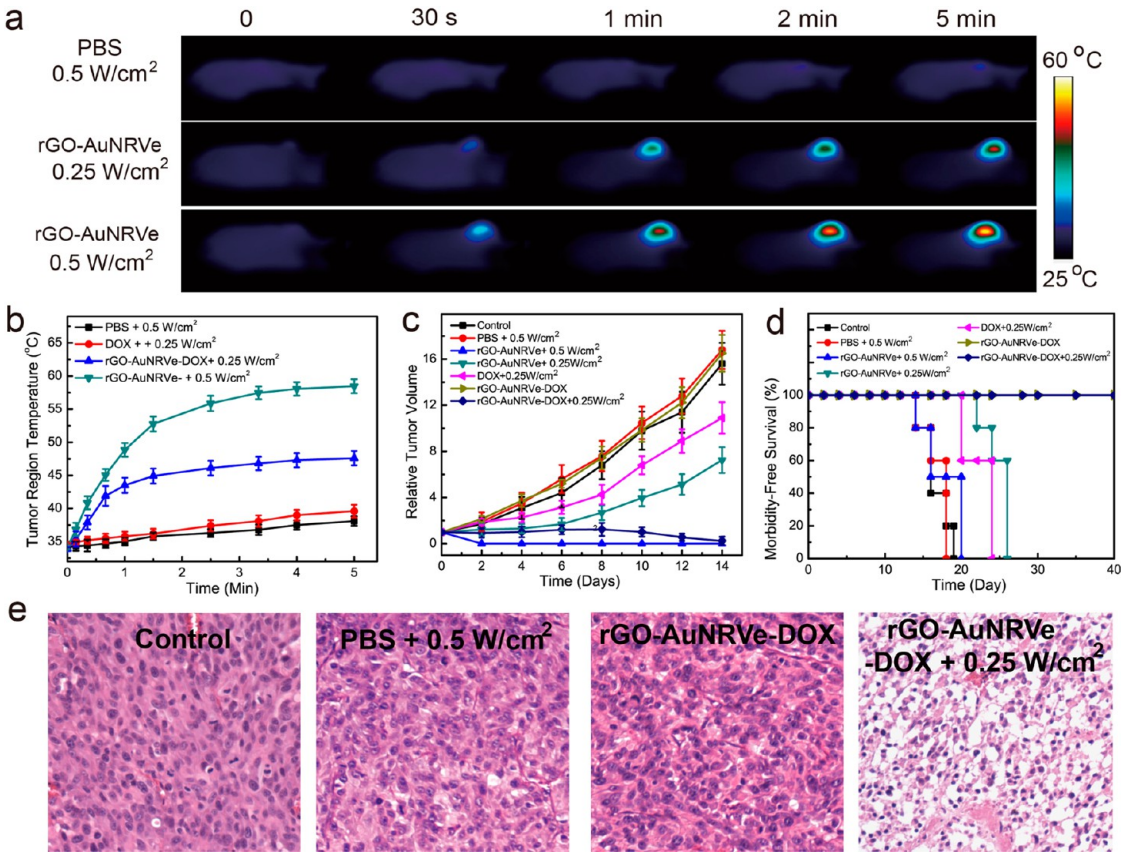

Figure 6. Synergistic chemo-photothermal effect on U87MG tumor-bearing mice of rGO-AuNRVe-DOX. Thermographic images (a) and temperature changes of the tumor region (b) of the mice treated with PBS, DOX, and rGO-AuNRVe-DOX irradiated with a 808 nm laser of different power densities for 5 min. (c) Relative tumor volume of the tumor-bearing mice after intravenous injection of the samples and exposed to the 808 nm laser at different power densities. Tumor volumes were normalized to their initial sizes. (d) Survival curves of mice bearing U87MG tumor after various treatments. (e) Images of H&E-stained tumor sections harvested from the tumor-bearing mice treated with PBS and rGO-AuNRVe-DOX with or without laser irradiation.

of rGO-AuNRVe and its high surface density PEG, providing relatively long circulation time for passive tumor accumulation of the vesicle. After intravenous injection of rGO-AuNRVe, the tumor uptake of the hybrid vesicle increased from 0.79% at 1 h to 3.68% ID/g at 6 h and reached ~9.7% ID/g at 24 h and still ~8.5% ID/g at 52 h (Figure 5d,e). The accumulation efficiency of the hybrid vesicle in the tumor was higher than the previously reported large PEGylated AuNR,[37] thus representing a more effective tumor accumulation and localized cancer therapy.

***In Vivo* Integrated Chemo-photothermal Therapy by Small Hybrid Vesicles.** The *in vivo* photothermal and combined chemo-photothermal therapy performance of the rGO-AuNRVe-DOX was further examined. The GO-AuNRVe-DOX was intravenously injected into the mice when the tumor volume reached ~60 mm^3. To demonstrate the integrated chemo-photothermal effect *in vivo*, rGO-AuNRVe and free DOX at the same dosage, as well as PBS, were used as controls. On the basis of the maximum tumor accumulation of the rGO-AuNRVe at 24 h postinjection from the PET and PA results, the entire tumor region was then irradiated with a 808 nm laser at a power density of 0.25 or 0.5 W/cm^2. Figure 6a shows the thermal images of the tumor region of mice treated with rGO-AuNRVe and exposed to the 808 nm laser. The average temperature of the tumor region rapidly increased to 57 °C after treatment with the 808 nm laser at 0.5 W/cm^2 (Figure 6a,b). The tumor region of the PBS-treated mice exhibited an increase of ~2 °C after laser irradiation. No temperature change of the surrounding tissue was observed without laser irradiation. Due to the excellent photothermal property of rGO-AuNRVe, the tumor growth of rGO-AuNRVe with the laser at 0.5 W/cm^2 was completely inhibited with no reoccurrence (Figure S12). Furthermore, mice treated with rGO-AuNRVe and laser (0.5W/cm^2) irradiation survived over 40 days without a single death, as displayed in Figure 6d. In contrast, the rGO-AuNRVe-treated mice without laser irradiation exhibited a tumor growth rate and an average life span (14−20 days) similar to the control or PBS-treated mice.

To further investigate the combined chemo-photothermal therapy potential of rGO-AuNR-DOX *in vivo*, we reduced the power density of the laser to 0.25 W/cm^2. As shown in Figure 6a,b, the average

temperature of the tumor region of the mice reached ~45 °C. This temperature is high enough to trigger the disruption of the vesicle, leading to the release of DOX and rGO-DOX. The rGO-AuNRVe vesicle did not show any difference in the therapeutic efficacy during the first 5 days after irradiation at 0.25 W/cm^2 with or without DOX. Probably the intracellular uptake of rGO-AuNRVe is not essential for an efficient photothermal therapy. However, this uptake was an essential step for the following acid-triggered DOX release. The delay of tumor growth in the rGO-AuNRVe-DOX-treated mice confirmed the synergistic therapeutic effect of the *in vivo* integrated chemo-photothermal therapy *via* rGO-AuNRVe-DOX, while the rGO-AuNRVe-treated mice had continued tumor growth. Importantly, mice in the control groups with a single treatment (free DOX, rGO-AuNRVe + 0.25 W/cm^2) had an average life span of 20−26 days, while mice in the treated group (rGO-AuNRVe-DOX + 0.25 W/cm^2) were almost tumor-free after treatment and survived over 40 days without a single death (Figure 6d). As shown in Figure 6e, the tumor tissue section under treatment with rGO-AuNRVe-DOX and laser irradiation showed a more severe cancer necrosis and fewer cancer cells. However, the mice treated with PBS and laser irradiation or rGO-AuNRVe-DOX without laser irradiation did not exhibit any tumor necrosis. No significant body weight drop was noticed during this period of observation (Figure S13). On the other hand, no noticeable signs of organ damage or inflammatory lesions were observed in several major organs collected at day 9 from mice treated with rGO-AuNRVe-DOX with or without laser irradiation (Figure S14). These results suggest that the biodegradable rGO-AuNRVe-DOX exhibit an excellent synergistic chemo-photothermal effect and biocompatibility, thus warranting further studies in different tumor models and possible clinical translation to treat cancer patients with tumor accessible by light.

CONCLUSION

In summary, we introduced a new class of hybrid rGO-loaded ultrasmall plasmonic AuNRVes, which showed excellent photothermal and photoacoustic properties, due to the response of rGO and the plasmonic gold nanoshell when irradiated with an NIR laser. One key finding is that DOX and DOX-loaded rGO could both be encapsulated into the hybrid vesicle, resulting in a dual photo- and acid-responsive DOX release pattern, useful for a remote-controlled drug release. The relatively small size of the vesicle (~65 nm) allowed excellent passive accumulation of the hybrid vesicle in the tumor when injected intravenously into tumor-bearing mice. The tumor region also exhibited a considerable PA signal, due to the high accumulation of the hybrid vesicle in the tumor region. These properties allowed visualization of the shape and size of the tumor, the adjustment of the NIR laser spot to cover the entire tumor region, and the laser power density to maximize the photothermal effect and minimize the side effects on the surrounding tissue. Using DOX released from vesicular cavity and from the rGO surface combined with low-power NIR laser-induced photothermal therapy using hybrid rGO-AuNRVes showed a complete ablation of the tumor, thus suggesting a synergistic effect of the dual chemo-photothermal therapy.

EXPERIMENTAL SECTION

Synthesis of Ultrasmall Amphiphilic Gold Nanorods Coated with PEG and PLGA (AuNR@PEG/PLGA). A 2 mL solution of CTAB-stabilized AuNRs was concentrated to 20 μL by centrifugation at 8000*g* for 20 min. Afterward a mixture of DMF (0.5 mL), 5 mg of PEG-SH (M_n = 5000), and 6 mg of PLGA-SH (M_n = 6000) in DMF (2 mL) was rapidly added into the obtained AuNR@CTAB solution. The mixture was then sonicated for 2 min and stirred at 50 °C for 4 h to ensure enough ligand exchange. The as-prepared AuNR coated with PEG and PLGA (AuNR@PEG/PLGA) was purified by five times repeated centrifugation and washed with chloroform. The AuNR@PEG/PLGA was dispersed in chloroform at 4 °C for subsequent use.

Preparation of rGO-Loaded Ultrasmall Gold Nanorod Vesicles. rGO-AuNRVes were prepared using a double-emulsion water-in-oil-in-water ($W_1/O/W_2$) method. Briefly, 0.4 mg of rGO-PEG was dissolved into 0.12 mL of DI (distilled) water (internal aqueous phase, W_1) and then added to 1 mL of chloroform (oil phase, O) containing 5 mg of AuNR@PEG/PLGA. The primary W_1/O emulsion was prepared by pulsed sonication for 1 min. This primary emulsion (W1/O) was immediately poured into 5 mL of 2% (w/v) PVA aqueous solution (re-emulsification solution, W_2) and further homogenized for 1 min at 6500 rpm to produce a $W_1/O/W_2$ double emulsion. The emulsion was further stirred at room temperature for 12 h to evaporate the oil phase. After the solution became clear, the resulting rGO-loaded vesicles were purified by centrifugation (3500*g*, 5 min) and dispersed in DI water.

Preparation of DOX-Loaded Ultrasmall Hybrid Gold Nanorod Vesicles (rGO-AuNRVe-DOX). To prepare DOX-loaded vesicles, rGO-PEG-DOX and DOX in water (W_1) and AuNR@PEG/PLA in chloroform were mixed and sonicated for 2 min to form a W_1/O emulsion. Afterward, the emulsion was immediately added into 5 mL of PVA solution and stirred for 12 h at room temperature. When the chloroform was completely evaporated, the solution became clear and the DOX-loaded hybrid vesicles were purified by centrifugation and finally dispersed in water. The loading content and efficiency were calculated by testing the characteristic UV absorbance of DOX at 485 nm.

Photothermal Effect of the Hybrid Vesicle Irradiated with an NIR Laser. A 0.5 mL amount of rGO-loaded vesicles and vesicle aqueous solution in a 1 mL tube was irradiated with an 808 nm laser at different power densities for 5 min. The spot size of the laser was adjusted to cover the entire solution surface. The thermal images and temperature increase of the aqueous solutions were recorded by using an infrared thermal camera. The plasmonic AuNR@PEG/PLGA vesicle aqueous solution and water as control experiments were also treated in the same conditions.

NIR Laser- and Acid-Triggered DOX Release. To investigate the NIR laser- and acid-triggered DOX release behaviors, 2 mL of the rGO-AuNRVe aqueous solution was transferred into one plastic dialysis tube with a membrane (MW cutoff: 3000 Da). The tube was then immersed in a 25 mL glass bottle filled with 15 mL of DI water. The NIR laser-triggered DOX release experiment was

carried out with 808 nm laser irradiation at a power density of 0.25 W/cm^2 for 3 min. For acid-triggered DOX release, the solution in a glass bottle was adjusted to pH = 5.0 by adding a 1 M HCl solution. The amount of released DOX at different times was calculated by testing the UV absorbance of the DOX at 485 nm.

***In Vitro* Photothermal Therapy of rGO-AuNRVe.** A standard cell counting kit-8 was utilized to analyze the cytotoxicity of rGO-AuNRVes following a general protocol. Briefly, U87MG human glioblastoma cells were seeded in a 96-well plate (1×10^4 cells/well). After incubation at 37 °C for 24 h, rGO-AuNRVes with a final concentration of 0.6 nM of gold nanorods were added and incubated for 3 h, the cells were then washed with PBS, and 100 μL of fresh medium was added. The cells were exposed to an 808 nm laser at different power densities for 5 min, respectively. After incubation for another 24 h, the viability of cancer cells was examined using the standard CCK-8 assay. All experiments were done in triplicate, and results were averaged.

***In Vitro* DOX Release of rGO-AuNRVe-DOX.** To monitor the intracellular DOX release by fluorescence imaging, the cells were treated with rGO-AuNRVe-DOX and irradiated with a laser at a power density of 0.25 W/cm^2 for 3 min. The cell nuclei of U87 MG cells were counterstained with Hoechst 33342. The fluorescence signal of DOX was detected at different time points using wideband blue excitation (450−480 nm) provided by a mercury lamp, a long-pass dichroic filter (500 nm), and a band-pass emission filter (590−630 nm).

***In Vitro* Integrated Chemo-photothermal Therapy of U87MG Cells Incubated with rGO-AuNRVe-DOX.** U87MG human glioblastoma cells were first seeded in a 96-well plate (1×10^4 cells/well). For integrated chemo-photothermal therapy, rGO-AuNRVe-DOX and free DOX of the same dosage of DOX were added into a 96-well plate. After incubation for 3 h, the cells were then washed with PBS, and 100 μL of fresh medium was added. The cells were irradiated with or without an 808 nm laser at a power density of 0.25 W/cm^2 for 5 min, respectively. After incubation for another 24 h, the viability of cancer cells was examined using the standard CCK-8 assay. All experiments were done in triplicate, and the results were averaged.

Preparation of Radioactive [^{64}Cu]-Labeled Plasmonic Vesicles. To prepare radiometal [^{64}Cu]-doped rGO-AuNRVes, 4 μL of $^{64}CuCl_2$ was premixed with 1.2 mg of Na-ascorbate (in 0.1 M borate buffer pH 8.6). Then 200 μL of rGO-AuNRVe (0.8 mg/mL) was added. The mixture was incubated at 37 °C for 1 h. The resulting [^{64}Cu]-labeled vesicles were purified by centrifugation (4000*g*, 5 min) three times to remove the unreacted [^{64}Cu] and excess amount of reagents. The purified [^{64}Cu]-labeled vesicles were finally dispersed in PBS. The labeling efficiency was determined by using instant thin-layer chromatography (ITLC) plates and 0.1 M citric acid pH 5 as an eluent.

***In Vivo* Photoacoustic Imaging.** The tumor was grown by inoculating 100 μL of U87MG cells with the concentration of 1×10^6 cells in PBS into the right shoulder of each nude mouse (female, 7 weeks old) under anesthesia. After the tumor volume reached ~60 mm^3, 200 μL of rGO-AuNRVes (0.5 mg/mL) was injected intravenously into the tumor-bearing mice. The PA image of the whole tumor region was scanned by using the VisualSonic Vevo 2100 LAZR system (40 MHz, 256-element linear array transducer) at 0, 2, 6, and 24 h postinjection. The AuNRVe was selected as the control sample.

***In Vivo* PET Imaging.** For the *in vivo* PET imaging experiment, 200 μL of ^{64}Cu-labeled rGO-AuNRVe was intravenously injected into the mice when the tumor volume reached ~60 mm^3. The whole-body PET scans and data calculation were processed by using an Inveon Micro PET scanner (Siemens Medical Solutions) at predetermined time intervals after injection.

***In Vivo* Combined Chemo-photothermal Cancer Therapy.** The photothermal and combined chemo-photothermal therapy effect *in vivo* was investigated by U87MG-tumor-bearing mice when the tumor volume reached ~60 mm^3. Six groups of mice, including (1) PBS only; (2) PBS + laser irradiation; (3) rGO-loaded hybrid vesicles only; (4) vesicles with laser irradiation; (5) rGO-DOX-loaded hybrid vesicles with laser irradiation; and (6) DOX, with five to six mice per group were used. At 24 h postinjection, the U87MG tumors on the mice were exposed to an 808 nm laser at a power density of 0.25 W/cm^2 for 5 min. A thermal camera was used to record the temperature images and changes of the tumor region during the laser treatment process. A digital caliper was employed to measure the tumor size at 2-day intervals after the laser irradiation. After laser irradiation, a caliper was applied to measure the dimensions of the tumor at various time points. The tumor volume V (mm^3) was calculated based on the formula $V = LW^2/2$, where L and W refer to the length and width of the tumor in millimeters.

Conflict of Interest: The authors declare no competing financial interest.

Supporting Information Available: The Supporting Information is available free of charge on the ACS Publications website at DOI: 10.1021/acsnano.5b03804.

^{1}H NMR, GPC, TEM, and TGA measurements and properties analysis of the small amphiphilic gold nanorods and hybrid rGO-loaded plasmonic vesicles (PDF)

Acknowledgment. This work was supported by a research program of China-Japan Union Hospital of Jilin University and intramural research program of the National Institute of Biomedical Imaging and Bioengineering (NIBIB), National Institutes of Health (NIH).

REFERENCES AND NOTES

1. Murphy, C. J.; Gole, A. M.; Stone, J. W.; Sisco, P. N.; Alkilany, A. M.; Goldsmith, E. C.; Baxter, S. C. Gold Nanoparticles in Biology: Beyond Toxicity to Cellular Imaging. *Acc. Chem. Res.* **2008**, *41*, 1721–1730.
2. Anker, J. N.; Hall, W. P.; Lyandres, O.; Shah, N. C.; Zhao, J.; Van Duyne, R. P. Biosensing with Plasmonic Nanosensors. *Nat. Mater.* **2008**, *7*, 442–453.
3. Yavuz, M. S.; Cheng, Y.; Chen, J.; Cobley, C. M.; Zhang, Q.; Rycenga, M.; Xie, J.; Kim, C.; Song, K. H.; Schwartz, A. G.; et al. Gold Nanocages Covered by Smart Polymers for Controlled Release with Near-Infrared Light. *Nat. Mater.* **2009**, *8*, 935–939.
4. Saha, K.; Agasti, S. S.; Kim, C.; Li, X.; Rotello, V. M. Gold Nanoparticles in Chemical and Biological Sensing. *Chem. Rev.* **2012**, *112*, 2739–2779.
5. Li, W.; Chen, X. Gold Nanoparticles for Photoacoustic Imaging. *Nanomedicine* **2015**, *10*, 299–320.
6. Mayer, K. M.; Hafner, J. H. Localized Surface Plasmon Resonance Sensors. *Chem. Rev.* **2011**, *111*, 3828–3857.
7. Halas, N. J.; Lal, S.; Chang, W.-S.; Link, S.; Nordlander, P. Plasmons in Strongly Coupled Metallic Nanostructures. *Chem. Rev.* **2011**, *111*, 3913–3961.
8. Giannini, V.; Fernández-Domínguez, A. I.; Heck, S. C.; Maier, S. A. Plasmonic Nanoantennas: Fundamentals and Their Use in Controlling the Radiative Properties of Nanoemitters. *Chem. Rev.* **2011**, *111*, 3888–3912.
9. Huang, P.; Lin, J.; Li, W.; Rong, P.; Wang, Z.; Wang, S.; Wang, X.; Sun, X.; Aronova, M.; Niu, G.; et al. Biodegradable Gold Nanovesicles with an Ultrastrong Plasmonic Coupling Effect for Photoacoustic Imaging and Photothermal Therapy. *Angew. Chem., Int. Ed.* **2013**, *52*, 13958–13964.
10. Song, J.; Pu, L.; Zhou, J.; Duan, B.; Duan, H. Biodegradable Theranostic Plasmonic Vesicles of Amphiphilic Gold Nanorods. *ACS Nano* **2013**, *7*, 9947–9960.
11. Song, J.; Fang, Z.; Wang, C.; Zhou, J.; Duan, B.; Pu, L.; Duan, H. Photolabile Plasmonic Vesicles Assembled from Amphiphilic Gold Nanoparticles for Remote-Controlled Traceable Drug Delivery. *Nanoscale* **2013**, *5*, 5816–5824.
12. Song, J.; Cheng, L.; Liu, A.; Yin, J.; Kuang, M.; Duan, H. Plasmonic Vesicles of Amphiphilic Gold Nanocrystals: Self-Assembly and External-Stimuli-Triggered Destruction. *J. Am. Chem. Soc.* **2011**, *133*, 10760–10763.
13. Song, J.; Zhou, J.; Duan, H. Self-Assembled Plasmonic Vesicles of SERS-Encoded Amphiphilic Gold Nanoparticles for Cancer Cell Targeting and Traceable Intracellular Drug Delivery. *J. Am. Chem. Soc.* **2012**, *134*, 13458–13469.
14. He, J.; Huang, X.; Li, Y.-C.; Liu, Y.; Babu, T.; Aronova, M. A.; Wang, S.; Lu, Z.; Chen, X.; Nie, Z. Self-Assembly of

Amphiphilic Plasmonic Micelle-Like Nanoparticles in Selective Solvents. *J. Am. Chem. Soc.* **2013**, *135*, 7974–7984.
15. Huang, X. H.; El-Sayed, I. H.; Qian, W.; El-Sayed, M. A. Cancer Cell Imaging and Photothermal Therapy in the Near-infrared Region by Using Gold Nanorods. *J. Am. Chem. Soc.* **2006**, *128*, 2115–2120.
16. Hubbell, J. A.; Chilkoti, A. Nanomaterials for Drug Delivery. *Science* **2012**, *337*, 303–305.
17. Zhang, W.; Guo, Z. Y.; Huang, D. Q.; Liu, Z. M.; Guo, X.; Zhong, H. Q. Synergistic Effect of Chemo-Photothermal Therapy Using PEGylated Graphene Oxide. *Biomaterials* **2011**, *32*, 8555–8561.
18. Kim, H.; Namgung, R.; Singha, K.; Oh, I.-K.; Kim, W. J. Graphene Oxide−Polyethylenimine Nanoconstruct as a Gene Delivery Vector and Bioimaging Tool. *Bioconjugate Chem.* **2011**, *22*, 2558–2567.
19. Yang, K.; Hu, L.; Ma, X.; Ye, S.; Cheng, L.; Shi, X.; Li, C.; Li, Y.; Liu, Z. Multimodal Imaging Guided Photothermal Therapy using Functionalized Graphene Nanosheets Anchored with Magnetic Nanoparticles. *Adv. Mater.* **2012**, *24*, 1868–1872.
20. Zhu, Y.; Murali, S.; Cai, W.; Li, X.; Suk, J. W.; Potts, J. R.; Ruoff, R. S. Graphene-based Materials: Graphene and Graphene Oxide: Synthesis, Properties, and Applications. *Adv. Mater.* **2010**, *22*, 3906–3924.
21. Han, C.; Zhang, Z.; Xu, H.; Li, J.; Xie, G.; Chen, R.; Zhao, Y.; Huang, W. Controllably Tuning Excited-State Energy in Ternary Hosts for Ultralow-Voltage-Driven Blue Electrophosphorescence. *Angew. Chem., Int. Ed.* **2012**, *51*, 10104–10108.
22. Moon, H.; Kumar, D.; Kim, H.; Sim, C.; Chang, J.-H.; Kim, J.-M.; Kim, H.; Lim, D.-K. Amplified Photoacoustic Performance and Enhanced Photothermal Stability of Reduced Graphene Oxide Coated Gold Nanorods for Sensitive Photoacoustic Imaging. *ACS Nano* **2015**, *9*, 2711–2719.
23. Zhu, X.; Shi, L.; Schmidt, M. S.; Boisen, A.; Hansen, O.; Zi, J.; Xiao, S.; Mortensen, N. A. Enhanced Light−Matter Interactions in Graphene-Covered Gold Nanovoid Arrays. *Nano Lett.* **2013**, *13*, 4690–4696.
24. Zhang, P.; Guo, Y. Surface-Enhanced Raman Scattering Inside Metal Nanoshells. *J. Am. Chem. Soc.* **2009**, *131*, 3808–3809.
25. Ali, M. R. K.; Snyder, B.; El-Sayed, M. A. Synthesis and Optical Properties of Small Au Nanorods Using a Seedless Growth Technique. *Langmuir* **2012**, *28*, 9807–9815.
26. Meng, F. T.; Ma, G. H.; Qiu, W.; Su, Z. G. W/O/W Double Emulsion Technique Using Ethyl Acetate As Organic Solvent: Effects of Its Diffusion Rate on the Characteristics of Microparticles. *J. Controlled Release* **2003**, *91*, 407–416.
27. Odom, T. W.; Schatz, G. C. Introduction to Plasmonics. *Chem. Rev.* **2011**, *111*, 3667–3668.
28. Mallidi, S.; Luke, G. P.; Emelianov, S. Photoacoustic Imaging in Cancer Detection, Diagnosis, and Treatment Guidance. *Trends Biotechnol.* **2011**, *29*, 213–221.
29. Sahu, A.; Choi, W. I.; Lee, J. H.; Tae, G. Graphene Oxide Mediated Delivery of Methylene Blue for Combined Photodynamic and Photothermal Therapy. *Biomaterials* **2013**, *34*, 6239–6248.
30. Sherlock, S. P.; Tabakman, S. M.; Xie, L.; Dai, H. Photothermally Enhanced Drug Delivery by Ultrasmall Multifunctional FeCo/Graphitic Shell Nanocrystals. *ACS Nano* **2011**, *5*, 1505–1512.
31. Liu, Z.; Robinson, J. T.; Sun, X.; Dai, H. PEGylated Nanographene Oxide for Delivery of Water-Insoluble Cancer Drugs. *J. Am. Chem. Soc.* **2008**, *130*, 10876–10877.
32. Kim, H.; Lee, D.; Kim, J.; Kim, T.-i.; Kim, W. J. Photothermally Triggered Cytosolic Drug Delivery via Endosome Disruption Using a Functionalized Reduced Graphene Oxide. *ACS Nano* **2013**, *7*, 6735–6746.
33. Zhang, X.-Q.; Lam, R.; Xu, X.; Chow, E. K.; Kim, H.-J.; Ho, D. Multimodal Nanodiamond Drug Delivery Carriers for Selective Targeting, Imaging, and Enhanced Chemotherapeutic Efficacy. *Adv. Mater.* **2011**, *23*, 4770–4775.
34. Kelkar, S. S.; Reineke, T. M. Theranostics: Combining Imaging and Therapy. *Bioconjugate Chem.* **2011**, *22*, 1879–1903.
35. Appel, A. A.; Anastasio, M. A.; Larson, J. C.; Brey, E. M. Imaging Challenges in Biomaterials and Tissue Engineering. *Biomaterials* **2013**, *34*, 6615–6630.
36. Kim, C.; Favazza, C.; Wang, L. V. *In Vivo* Photoacoustic Tomography of Chemicals: High-Resolution Functional and Molecular Optical Imaging at New Depths. *Chem. Rev.* **2010**, *110*, 2756–2782.
37. Sun, X.; Huang, X.; Yan, X.; Wang, Y.; Guo, J.; Jacobson, O.; Liu, D.; Szajek, L. P.; Zhu, W.; Niu, G.; et al. Chelator-Free ^{64}Cu-Integrated Gold Nanomaterials for Positron Emission Tomography Imaging Guided Photothermal Cancer Therapy. *ACS Nano* **2014**, *8*, 8438–8446.
38. Sun, X.; Huang, X.; Guo, J.; Zhu, W.; Ding, Y.; Niu, G.; Wang, A.; Kiesewetter, D. O.; Wang, Z. L.; Sun, S.; et al. Self-Illuminating ^{64}Cu-Doped CdSe/ZnS Nanocrystals for *In Vivo* Tumor Imaging. *J. Am. Chem. Soc.* **2014**, *136*, 1706–1709.